Detailed 3D Seismic Velocity Structure of the Prague, Oklahoma Fault Zone and the Implications for Induced Seismicity

Lipeng He[1,2], Qimin Wu[1,3,*], Xiaowei Chen[1], Xinlei Sun[4], Zhen Guo[2] and Yongshun John Chen[2,*]

[1]School of Geosciences, University of Oklahoma, Norman, OK, USA.

[2]Department of Ocean Science and Engineering, Southern University of Science and Technology, Shenzhen, Guangdong, China.

[3]Lettis Consultants International, Inc., Concord, CA, USA.

[4]International Center for Planetary Science, College of Geosciences, Chengdu University of Technology

Corresponding authors: Qimin Wu (wu@lettisci.com), Yongshun John Chen (johnyc@sustech.edu.cn)

Key Points:

- We develop a fine fault zone velocity structure for the 2011 Mw 5.7 Prague earthquake and relocate the earthquakes using the 3D models.
- The results depict the Meeker-Prague Fault that hosted the majority of the larger events in the Prague sequence.
- We propose a conceptual model that links velocity structure to the triggering process of the Prague sequence due to wastewater injection.

Abstract

The 2011 Mw 5.7 Prague earthquake is the second largest induced earthquake in Oklahoma, and occurred after decades of wastewater disposal. The local geological structure that led to the triggering of this large earthquake is not well understood. In this study, tomographic inversion of seismic data recorded by a dense local seismic network resulted in a high-resolution 3D velocity model with three major layers. The model clearly illuminates the geometry and characteristics of the Meeker-Prague Fault that hosted the 2011 Prague sequence. A conceptual model is proposed to link the tomographic structure to the triggering process of the sequence. The low-permeability second layer at ~1.5-3.5 km may be the key that delays the occurrence of the first sizeable earthquake after decades of wastewater injection. However, a low-shear-velocity zone within this layer at the intersection of two major faults could have provided a fluid pathway to facilitate downward fluid propagation.

Plain Language Summary

The recent surge of seismicity in the central United States since 2008 has largely been attributed to wastewater disposal from oil and gas production. The 6 November 2011 Mw 5.7 earthquake near Prague, is the second largest earthquake ever recorded instrumentally in the state of Oklahoma. Previous studies mainly focused on the characterization of seismicity in the 2011 Prague earthquake sequence and found that the majority of earthquakes occurred along the Meeker-Prague fault, which is a ~20 km splay fault off the Wilzetta fault zone. In this study, we apply the seismic traveltime tomography technique on data recorded by a dense local seismograph network to image the fine upper crustal velocity structure in the Prague fault zone. Our results clearly mapped zones with significant velocity anomalies in the fault zone compared to the surrounding area. And the velocity anomalies coincide with the clusters of seismicity, indicating that fluid injection probably played an important role in altering the properties of the fault zone and therefore promoting the occurrence of earthquakes. This study highlights that it is critical to investigate the fault zone structure to advance our understanding of the process of pore pressure diffusion and fluid migration in triggering of induced seismicity.

1 Introduction

The unprecedented increase in the seismicity rate in the central United States (CUS) since 2008 has largely been attributed to the large volume of wastewater disposal from oil and gas production (Ellsworth, 2013; Keranen & Weingarten, 2018). In Oklahoma, several significant induced earthquakes have occurred since 2011, including the 2011 Mw 5.7 Prague earthquake and the 2016 Mw 5.8 Pawnee earthquake, both of which caused considerable damage in the epicentral regions (Keranen et al., 2013; Yeck et al., 2016). Although the earthquake rate has been declining in Oklahoma since 2016, in part due to mandated reductions in rates for wastewater injection (Stewart & Ingelson, 2017), it remains well above background levels and puts the state at an elevated level of seismic hazards (Langenbruch & Zoback, 2016; Petersen et al., 2016; Petersen et al., 2017; Petersen et al., 2018).

It is generally accepted that the increase in pore fluid pressure associated with wastewater injection reduces the frictional resistance on pre-existing fault planes and thus promotes their reactivation. The fact that not all wells with high wastewater injection rates are linked to induced earthquakes, and that sometimes earthquakes occur near wells with low injection rates, indicates that induced seismicity depends both on the injection parameters and on the local geological

structures (Schultz et al., 2016; Shah & Keller, 2017). Regional studies on the crustal structures in Oklahoma indicate that moderate earthquakes tend to occur close to the boundaries of high- and low-seismic velocity zones that are interpreted as geological boundaries of different basement rock properties (Pei et al., 2018; Chai et al., 2021). The hydrological structure of the subsurface is important in controlling the spatial and temporal distributions of fluid pressure perturbations in the subsurface. Highly permeable fault zones facilitate pore pressure propagation and channel fluid flow to travel large distances from injection wells, potentially reaching critically stressed basement faults (e.g., Chiarabba et al., 2018; Shah & Keller, 2017). It is therefore critical to identify the structures that control pore pressure diffusion and fluid migration toward large active faults in order to advance our understanding of the triggering mechanisms of induced seismicity.

The 2011 Mw 5.7 Prague earthquake sequence was the first significant earthquake sequence that has been attributed to wastewater disposal in Oklahoma, which ruptured a previously unmapped portion of the Wilzetta Fault zone (WFZ) (Figure 1, Keranen et al., 2013; McMahon et al., 2017). The relocated seismicity and focal mechanisms suggest a complex fault zone with three primary faults, as defined by the Mw 4.8 foreshock, the Mw 5.7 mainshock, and the Mw 4.8 aftershock, respectively (Cochran et al., 2020; Keranen et al., 2013; McMahon et al., 2017; Pennington et al., 2021). Seismological analysis suggests that the Mw 5.7 mainshock ruptured an unmapped Meeker-Prague Fault (MPF, McMahon et al., 2017) that is optimally oriented in the stress field (Cochran et al., 2020). The onset of induced earthquakes is commonly observed soon after the initiation of fluid injection (e.g., Frohlich et al., 2011; Horton, 2012; Tan et al., 2020). However, the first notable earthquake (i.e., the Mw 4.8 foreshock) near Prague did not occur until 18 years after injection had commenced, and there is no clear temporal correlation between changes in wastewater disposal rates at the wells and the timing of the Prague sequence in late 2011 (Walsh & Zoback, 2015). The coseismic rupture of the Mw 5.7 mainshock is considerably heterogeneous consisting of multiple slip patches at depths ~3-9 km (Sun & Hartzell, 2014), indicating variable fault strength and stress conditions on the fault, which is consistent with the strong variability of stress drop estimates for the sequence (Pennington et al., 2021; Sumy et al., 2017; Wu et al., 2018). In addition, stress field analysis by Cochran et al. (2020) demonstrates that both optimally and unfavorably oriented faults were activated during the 2011 Prague sequence, which highlights the complex structure of the fault zone, as well as the significance of pore pressure changes in promoting the failure of the unfavorably oriented faults, in addition to the triggering by earthquake interaction through Coulomb stress transfer (e.g., Chen et al., 2017; Sumy et al., 2014). However, the mechanism that controls the timing and detailed failure process of the 2011 sequence and the relative contributions of fault zone structures and pore pressure changes due to injection remain unclear.

To shed light on the aforementioned scientific questions, in this study, we focus on the fine 3D structure of the fault system, and the role of fluids in the evolution of the Prague sequence. The new results presented here allow us to evaluate the link between the fault zone structure and the evolution of seismicity, providing new insights on the triggering processes of induced seismicity.

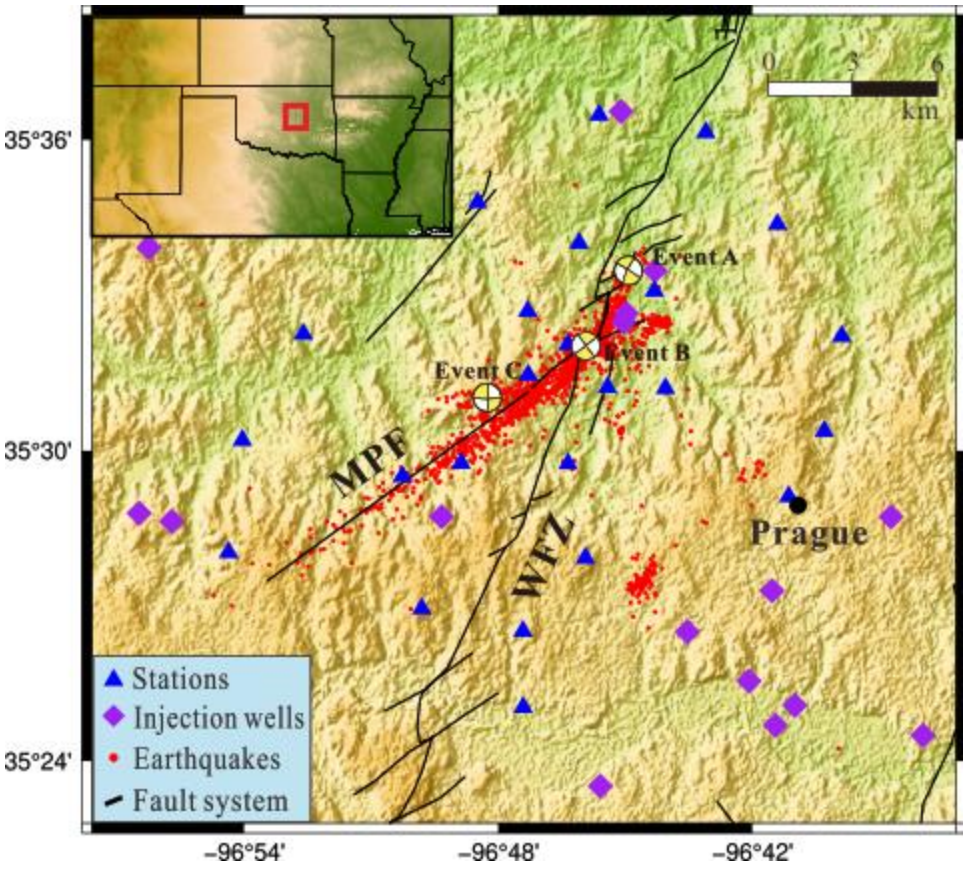

Figure 1. Topographic map of the Prague, Oklahoma. Inset map shows the location of the study area (red rectangle). Faults are marked with black solid lines. Blue triangles show the seismic stations and purple diamonds represent the wastewater injection wells. MPF: Meeker-Prague Fault, WFZ: Wilzetta Fault zone. Event A, B and C represent the Mw 4.8 foreshock (5 November 2011), the Mw 5.7 mainshock (6 November 2011) and the Mw 4.8 aftershock (8 November 2011), respectively (locations from USGS). Red dots denote the 1508 earthquake locations from the catalog by McMahon et al. (2017) between November 2011 and April 2012.

2 Data and Methods

Shortly after the Mw 4.8 foreshock on 5 November 2011, teams from the Program for Array Seismic Studies of the Continental Lithosphere (PASSCAL), Rapid Array Mobilization Program (RAMP), the University of Oklahoma (OU), and the United States Geological Survey (USGS) deployed 31 three-component temporary seismometers to monitor the following seismic activity near Prague (Figure 1, Sumy et al., 2014). We selected a subset of 1508 well-recorded earthquakes that were recorded by at least 5 stations from the template-matching derived catalog by McMahon et al. (2017), and manually picked P and S wave arrivals. We only used earthquakes with both P and S phase picks at five or more stations to facilitate a better comparison between Vp and Vs, and to ensure the reliability of the Vp/Vs (Zenonos et al., 2020). To further filter out low-quality data, we evaluated the distribution of the P and S wave travel times versus distance and fitted the data using least squares linear regression (Figure S1). Traveltime data that fall outside two standard deviations about the linear trend were considered outliers and were eliminated. Finally, we obtained 18,900 P wave and 18,900 S wave arrival times for further analyses.

We first use the HypoDD program (Waldhauser & Ellsworth, 2000; Figure S2, Text S1) to relocate the selected earthquakes using a 1D velocity model of Prague (Keranen et al., 2013), and then invert the selected P wave and S wave arrival times for 3D velocity models. The ray-paths for all data used in the tomography are presented in Figure S3. We adopt the Fast Marching tomography algorithm (FMTOMO, de Kool et al., 2006; Rawlinson et al., 2006, Text S2) to invert for both the Vp and Vs structures. For the determination of the Vp/Vs model, instead of simply taking the ratio of Vp and Vs models, we apply a modified version of the FMTOMO code to directly invert for Vp/Vs using S-P times following Zenonos et al. (2020), which has been demonstrated to produce more robust Vp/Vs model. The region of interest in this study is approximately 40 km (EW direction) by 30 km (NS direction), and extends from the ground surface to 16 km depth. The inversion converged after six iterations, and the root-mean-square of the traveltime residuals was reduced from 0.43 to 0.23 s for P arrivals and from 0.65 to 0.24 s for S arrivals for the final velocity model. Figure S4 shows the traveltime residuals after inversion for both P- and S-waves. The residuals are centered at 0 s with the majority falling within the range of -0.2 to 0.2 s, suggesting that the final model predicts the traveltimes quite well. Lastly, we relocat the earthquakes using our inverted 3D velocity models and the 3D version of HypoDD.

We perform checkerboard tests to evaluate the resolution of the 3D velocity models. In the checkerboard resolution tests, we set the input velocity perturbations at ±0.5 km/s relative to the reference model. The spatial resolution is about 2.5 km in both horizontal and vertical directions based on the results of the checkerboard tests. Figure S5, S6 and S7 show depth slices and cross-sectional views of the recovered models for Vp, Vs and Vp/Vs, respectively. These figures suggest that the models are well resolved at depths of 0-8 km.

3 Results

Figure 2 shows horizontal slices of Vp (left), Vs (middle), and Vp/Vs (right) models at various depths. In general, Vp and Vs models show similar patterns. At the surface (Figure 2a, b, c), low velocities with high Vp/Vs spread widely, including within the WFZ and along the MPF. The widespread low velocities near the surface are associated with the sedimentary layer in this region. In contrast, the low velocity anomalies at 4 km depth show more concentrated pattern that generally follows the trend of the MPF, and almost all earthquakes at this depth occurred within the low velocity zones (Figures 2d, e), which correlate remarkably well with the region of low Vp/Vs anomalies (Figure 2f). Similarly, a low Vp/Vs zone at 8 km depth correlates well with the low velocity anomalies and follows the trend of the MPF (Figure 2g, h and i). Notably, the most significant velocity anomalies, particularly Vp/Vs, occur at the intersection of WFZ and MPF (Figure 2), where the Mw 5.7 mainshock and the Mw 4.8 foreshock are located.

Figure 3 shows cross sections for the resulting Vp (Figures 3a, b), Vs (Figures 3c, d), and Vp/Vs (Figures 3e, f) models along two orthogonal profiles with profile AA' trending NE-SW along the MPF (Figure 2a). Based on the velocity profiles, we infer three layers in the fault zone with distinct velocity characteristics (Figure 3c).

The sedimentary layer is clearly outlined by low Vp and Vs at depths shallower than ~1.5 km across the entire study area ("Layer 1" in Figure 3c). This layer is also associated with high Vp/Vs, particularly around the fault zone (Figures 3e, f). The bottom of this layer varies at depth from about 1 to 2 km, consistent with the depth to the Arbuckle and Hunton formations obtained from well logs and electrical logs (Pennington et al., 2021). At "Layer 2" (Figure 3c), between ~1.5-3.5 km depth, the models are characterized by Vp and Vs with moderate velocity values and

relatively normal Vp/Vs. A notable low Vs anomaly (marked as "LSV" in Figure 3c) exists near the northeast end of the seismicity volume in "Layer 2", which connects the "Layer 1" and "Layer 3". "Layer 3", which is located right below the Arbuckle formation in the basement and hosted a majority of events including the Mw 5.7 mainshock, exhibits remarkable low Vp and Vs along with anomalously low Vp/Vs (Figure 3). Figure S8 shows three representative 1D vertical profiles along cross section AA' including one background profile, a second going through the low Vs anomaly LSV, and the third going through the low-velocity anomaly in Layer 3 but does not pass LSV.

To further investigate whether the three-layer upper crustal structure discussed above is a robust feature, we apply a synthetic reconstruction test based on a simplified 3D Vs model of the study area (Figure 3g, h). The synthetic model has a background Vs of 3.25 km/s, and consists of a low-velocity anomaly of 2.5 km/s from the surface to 1.5 km in "Layer 1", another low-velocity anomaly of "2.75" km/s at 3.5-8 km depth in "Layer 3", and a narrow cylindrical low-velocity anomaly of 2.75 km/s that connects "Layer 1" and "Layer 3" near the northwest edge of the anomalies (marked as "SLSV" in Figure 3g). We generate synthetic travel time data based on the source-receiver geometry, and obtain inverted velocity model following the same workflow. The inverted model agrees well with the input model in terms of both the shape and amplitude of the velocity anomalies (Figure 3h), suggesting that the layered structure is a robust feature. A similar input model without the "SLSV" feature was also tested, which further ensures that the recovered "SLSV" in Figure 3h was not an artifact caused by smearing effects (Figure S9).

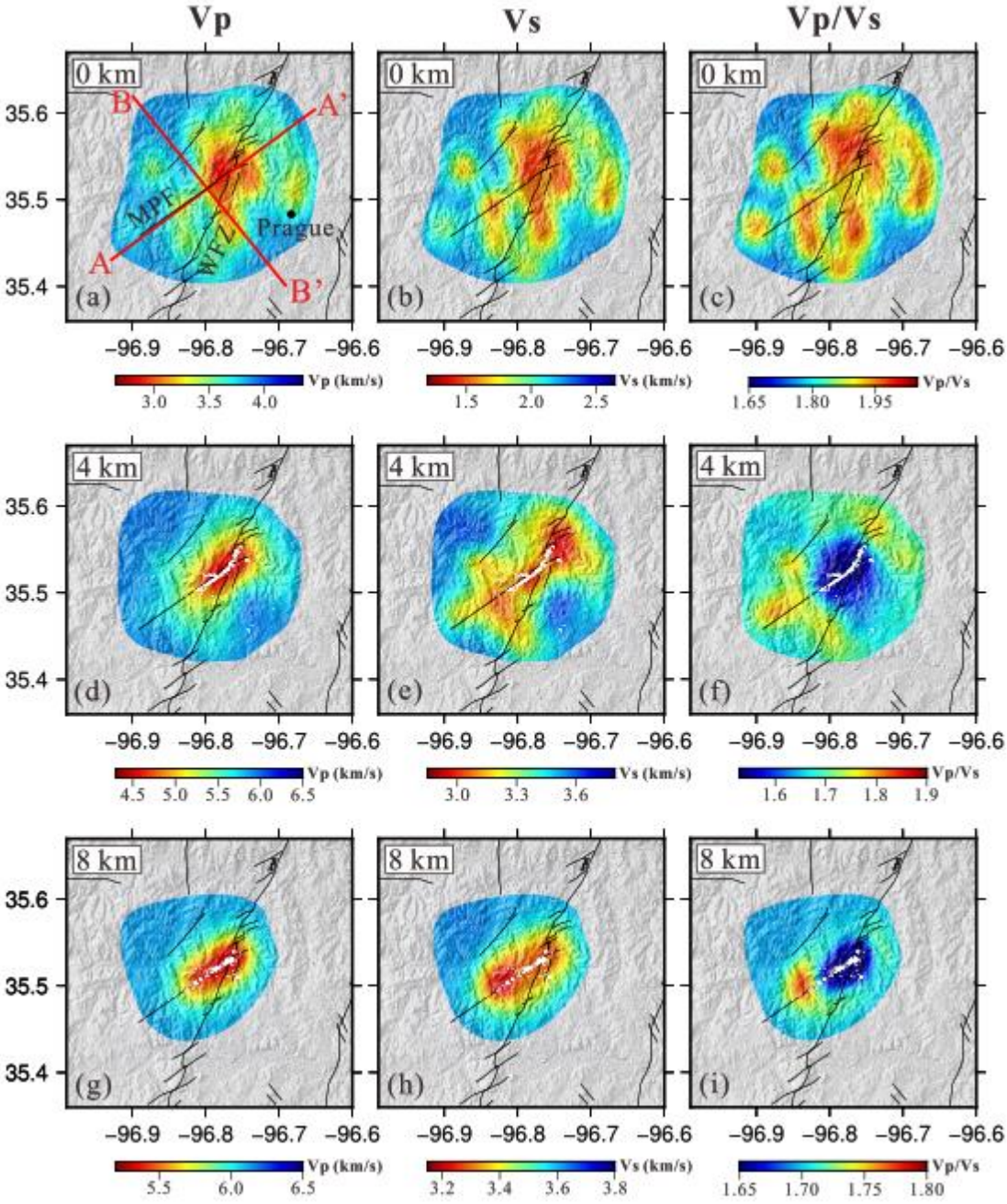

Figure 2. Map views of the final velocity models: Vp (left), Vs (middle), and Vp/Vs (right). Black lines mark the faults in study area and the two profiles are shown as red lines on Figure 2a. White dots are projected earthquakes from the relocated catalog using 3D velocity models within 1.5 km of the depth slices.

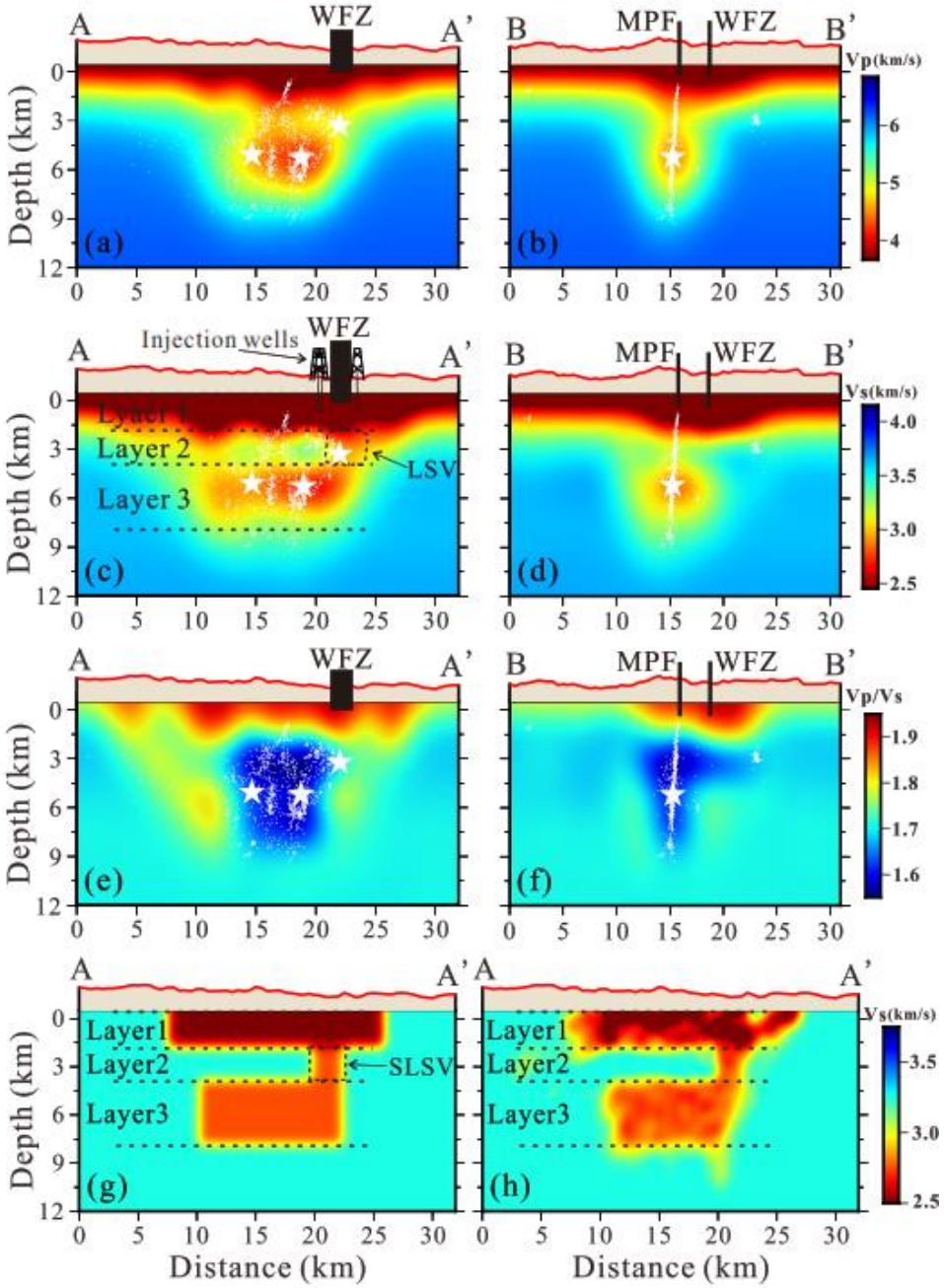

Figure 3. (**a-f**) Cross section along profiles AA' (left) and BB' (right). Top, middle, and bottom panels show the Vp, Vs, and Vp/Vs, respectively. White dots are projected earthquakes from the relocated catalog using 3D velocity models within 1.5 km of the cross sections and the Mw 5.7 mainshock, Mw 4.8 foreshock and Mw 4.8 aftershock are shown as white stars. (**g**) Synthetic input model with three layers. (**h**) Inverted model for the synthetic test.

4 Discussion

Induced earthquakes are generally interpreted as the reactivation of pre-existing faults due to stress changes caused by fluid injection (Ellsworth, 2013; Gupta, 2002). Thus, the detailed structure and morphology of the MPF is important for understanding induced seismicity in Prague. WFZ is the most significant mapped fault system near the Prague area, but the distribution of earthquakes (Figures 1, 2) suggests that the unmapped NE-oriented MPF, instead of the WFZ, is the primary host of the 2011 Prague sequence (Keranen et al., 2013; McMahon et al., 2017). Aeromagnetic Data reveals a correlation between low magnetic anomalies and MPF with strong heterogeneities within the fault zone (Shah & Crain, 2018). Yet, there has been no high-resolution tomographic studies to date at local scale to constrain the detailed morphology of MPF and its relationship with the Prague sequence.

Velocity variations in fault zones reflect the combined effects of lithology, crack density, porosity, and water content (e.g., He et al., 2018; Langenbruch & Zoback, 2016). Based on our 3D relocation of earthquakes (Figure S10) and velocity models, we infer that the MPF has a strike of about N45°E (Figure 2), which is consistent with the orientation of the MPF suggested by the aftershock distribution (McMahon et al., 2017). The 3D velocity models show near-vertical, low-velocity zones (Figures 3b, d) with low Vp/Vs (Figure 3f) occurring between 2.5 km and 8 km depth, coincident with the coseismic rupture of the mainshock and spatial extent of the aftershocks. In addition, the vertical variations of the velocity and Vp/Vs structures (e.g., "Layer 2" versus "Layer 3" in Figure 3c) suggest that small-scale complexities do exist within the fault zone, as previously recognized by Shah and Crain (2018). It should be noted that our model has a spatial resolution of ~2.5 kilometers, which prevents the identification of minor fault structures, such as the EW-trending fault branch outlined by the aftershocks of the Mw 4.8 aftershock on 8 November 2011 (Cochran et al., 2020; McMahon et al., 2017).

McMahon et al. (2017) shows that over 99.9% of the cumulative moment in the catalog was released below 2.6 km depth. Our updated earthquake relocations using 3D velocity models (Figures 2, 3 and S10) show that most earthquakes (including the Mw 5.7 mainshock) occurred within the imaged velocity anomalies. The 3D relocations are overall consistent with 1D relocations with relatively small changes, however, both 3D and 1D relocations show large shifts from the original locations (Figure S11). More significantly, all the larger earthquakes in this sequence ($Mw \geq 3.5$) occurred at depths of ~4-9 km of the MPF (Figure S12). Earthquake scaling laws indicate that these larger earthquakes could have been produced by a fault with the size of the MPF imaged by this study (e.g., Qin et al., 2019; Walsh & Zoback, 2015).

The shear and bulk modulus are different for saturated cracks with different aspect ratios, and the Vp/Vs anomalies can be related to different factors including water content, aspect ratio, and crack density (Lin & Shearer, 2009; Shearer, 1988). Our tomographic models reveal prominent high Vp/Vs in the sedimentary layer ("Layer 1" in Figure 3c), where large volume of wastewater has been injected into the Arbuckle group (Keranen et al., 2013), suggesting that the sedimentary layer is characterized by fluid-filled cracks with small aspect ratio in saturated carbonates (e.g., <0.01, Lin and Shearer, 2009; Shearer, 1988). The "Layer 2" has normal granite velocity values and relatively normal Vp/Vs, which indicates a relatively uniform structure and lower permeability. The intersection of the MPF and WFZ is marked as a low shear velocity zone, possibly indicating reduced fault strength.

The Vp/Vs at the MPF ("Layer 3" in Figure 3c) is approximately 1.6, which is around 8% lower than the background value of 1.73. This can be explained by fluid-filled cracks with high aspect ratio (Shearer, 1988; Takei, 2002), A 8% reduction in the Vp/Vs corresponds to a medium porosity of around 10% assuming an aspect ratio of 0.1 and an initial Vp/Vs of 1.73 (Lin & Shearer, 2009). Moreover, we apply the method of Lin and Shearer (2007) to estimate the situ Vp/Vs in "Layer 3" using P-wave and S-wave differential times (Figure S13, Text S3). This technique has high resolution for near-source Vp/Vs using high-precision differential times and a robust misfit function method. The consistency between the Vp/Vs (~1.6) estimated using differential travel-times and our tomography results highlights the reliability of our Vp/Vs estimates.

Due to the lack of seismicity and monitoring stations prior to the Prague sequence, it is impossible to infer the structure in earlier stage so as to provide a definite triggering process of the Prague sequence. Our 3D model represents the average upper crust structure during and following the Prague earthquake sequence. Figure 4 shows a 3D perspective view of the inverted Vs model. The isosurface of a Vs of 3 km/s forms a cylinder at depths of ~3.5-8 km, outlining the extent of the low-velocity “Layer 3” that extends upwards and connects to the sedimentary layer through a possible flow channel near the intersection of WFZ and MPF. Additional plots (Figures S14 and S15) and animations showing the 3D Vs isosurface structure from various viewing angles are included in the Supporting Information. Lateral variations of body wave velocities are widely observed worldwide in fault zones, whether associated with industrial activity or not, and are often related to fluids (Allam et al., 2014; Di Stefano et al., 2011; Lei & Zhao, 2009; Tan et al., 2020). In the current study, the resolved strong velocity and Vp/Vs anomalies at seismogenic depths define the extent of the possibly overpressurized volume influenced by fluid injection, which suggests that fluid-filled cracks may be present down at least 8 km in depth, and therefore, fluid may have played a key role in triggering the sequence.

Combining all the observations, we propose a simplified conceptual model for the development of the Prague sequence: Fluid injection into the three active injection wells within ~1.5 km of Event A (Figure 1) started since 1993, and extended into the deeper Arbuckle Group between ~1.3 and 2.1 km depth (Keranen et al., 2013). Since the Arbuckle Group comprises highly permeable reservoirs (Keranen et al., 2013), the wastewater quickly diffused into the surroundings (Shah & Keller, 2017), triggering some small earthquakes due to the increase in pore pressure. The relatively complete central Oklahoma granite group ("Layer 2" in Figure 3c, Shah & Keller, 2017) at depth ~1.5-3.5 km, which has a very low permeability, inhibits further downward wastewater penetration in general. Seismicity during this time period is therefore limited to the sedimentary layers and the uncovered preexisting MPF remains stable. The low-permeability of "Layer 2" maybe the main reason that the first sizeable earthquake did not occur until 18 years after the wastewater injection commenced (Keranen et al., 2013). As noted by Keranen & Weingarten (2018), the lack of induced seismicity in North Dakota is partially due to the low permeable layers above and below the injection layer, which supports our interpretation. However, as injection continues, at the intersection of the MPF and WFZ in "Layer 2" (marked as “LSV” in Figure 3c), the fault strength gradually decreases in response to increased pore pressure as wastewater accumulates. Then the density-driven pressure front migrates downward (Pollyea, et al., 2019) at this fault intersection. This process of downward diffusion resulted in increased pore pressure, decrease the fault strength, and may have induced the Mw 4.8 foreshock (Event A in Figure 4) in "Layer 2" (Keranen et al., 2013; Sumy et al., 2014).

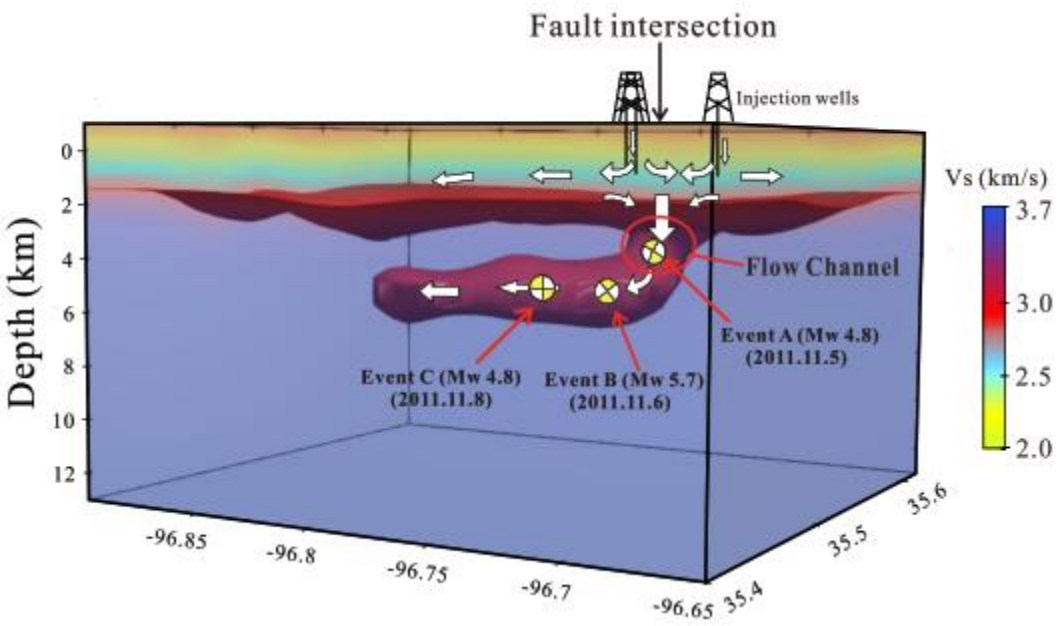

Figure 4. 3D visualization of the inverted Vs model. The isosurface of a Vs 3 km/s forms a cylinder at the depth of ~3.5-8 km and connects upward with the shallow part near in the fault intersection. The magnitude and location of Event A (Mw 4.8, at 3.1 km depth), B (Mw 5.7, at 5.2 km depth) and C (Mw 4.8, at 5.0 km depth) are from USGS. The white arrows indicate possible directions of fluid diffusion and the red circle marks the possible location of the flow channel.

The MPF is optimally oriented in the local stress field, and may have been critically stressed (Cochran et al., 2020; Qin et al., 2019). The stress interactions from foreshocks and accumulated pore pressure triggered a run-off rupture along the MPF, resulting in the Mw 5.7 mainshock (Event B in Figure 4). Numerical modeling suggests that critically stressed faults is more likely to have run-off ruptures that extends beyond pressurized zone (Gischig, 2015).

The rupture processes of Event A and B might have created a flow channel in "Layer 2" (Figure 4), allowing the wastewater to easily penetrate into the MPF. Subsequently, the combined effect of the Coulomb stress changes from Events A and B and the increased pore pressure promotes the failure of the Mw 4.8 aftershock (Event C in Figure 4) and later aftershocks (Sumy et al., 2014).

Based on our model, the low permeability of "Layer 2" and the limited pathway at the fault intersection for the downward fluid penetration are the two reasons for the significant delay of the first sizeable earthquake that occurred 18 years after the fluid injection started. An in-depth study of Layer 2, including assessment of lateral differences in lithology and structure, will be critical in understanding the triggering processes of the Prague sequence. In addition, smaller scale structures are evident but beyond the resolution of our tomographic models. Most of those secondary faults including the ones that hosted the Mw 4.8 foreshock and Mw 4.8 aftershock were found not optimally oriented for failure in the local stress field, which underlines the dominant effect of elevated pore fluid pressures, when compared with the small footprint of stress perturbations

caused by static and dynamic stress transfers (Brown et al., 2018), in promoting failure along those smaller faults that would otherwise remain inactivated in ambient stress field (Cochran et al., 2020). Our proposed conceptual model can provide valuable guidance for numerical simulations on induced seismicity with a particular target on the delayed mainshock occurrence as observed at Prague and the 2017 Mw 5.5 Pohang, Korea earthquake (Yeo et al., 2020)

5 Conclusions

In this study, we imaged fine upper crustal velocity structures in the fault zone of the 2011 Mw 5.7 Prague, Oklahoma earthquake using data from a dense local seismic network. The new models reveal a three-layer structure of the Prague fault zone: a sedimentary layer extending from the surface to a depth of ~1.5 km, comprised of fluid-filled cracks with small aspect ratio, followed underneath by a relatively uniform basement layer with low permeability at around 1.5-3.5 km depths, and then a layer in the basement with fluid-filled cracks of high aspect ratio at depths of around 3.5-8 km. Based on our obtained velocity models and relocated earthquake locations, we infer that the MPF ruptured in "Layer 3" and hosted the majority of the larger events in the Prague sequence including the Mw 5.7 mainshock. The low permeability of "Layer 2" is probably what delays the first sizeable earthquake (Mw 4.8 foreshock) after 18 years of wastewater injection. More importantly, the weak zone at the fault intersection had provided the focused pathway for the downward penetration of the injected fluids.

Acknowledgments

We are grateful to Dr. Zenonos for providing us the software to invert Vp/Vs. We thank the Editor Dr. Germán Prieto, the anonymous Associate Editor, and two anonymous reviewers for helpful reviews. This study was supported by USGS NEHRP grant G18AP00022. Figures were made using GMT (Wessel et al., 2019), Matplotlib (Hunter, 2007) and ParaView. The seismic waveforms were obtained from the Incorporated Research Institutions for Seismology (IRIS) Data Management Center (http://ds.iris.edu/wilber3/find_event).

Open Research

The data used and produced in this study including the phase picks, recloated catalog, inverted velocity models are available at https://zenodo.org/record/5501768.

References

Allam, A. A., Ben-Zion, Y., Kurzon, I., & Vernon, F. (2014). Seismic velocity structure in the Hot Springs and trifurcation areas of the San Jacinto Fault zone, California, from double-difference tomography. *Geophysical Journal International*, *198*(2), 978-999. https://doi.org/10.1093/gji/ggu176

Brown, M. R. M., & Ge, S. (2018). Small earthquakes matter in injection-induced seismicity. *Geophysical Research Letters*, 45, 5445 -5453. https://doi.org/10.1029/2018GL077472

Chai, C., Delorey, A. A., Maceira, M., Levandowski, W., Guyer, R. A., Zhang, H., et al. (2021). A 3D Full Stress Tensor Model for Oklahoma. *Journal of Geophysical Research: Solid Earth, 126*(4), e2020JB021113. https://doi.org/10.1029/2020JB021113

Chen, X., Nakata, N., Pennington, C., Haffener, J., Chang, J. C., and He, X. (2017). The Pawnee earthquake as a result of the interplay among injection, faults and foreshocks. *Scientific Reports*, *7*(1), 4945. https://doi.org/10.1038/s41598-017-04992-z

Chiarabba, C., De Gori, P., Cattaneo, M., Spallarossa, D., & Segou, M. (2018). Faults geometry and the role of fluids in the 2016–2017 Central Italy seismic sequence. *Geophysical Research Letters*, 45, 6963–6971. https://doi.org/10.1029/ 2018GL077485

Cochran, E. S., Skoumal, R. J., McPhillips, D., Ross, Z. E., & Keranen, K. M. (2020), Activation of optimally and unfavourably oriented faults in a uniform local stress field during the 2011 Prague, Oklahoma, sequence. *Geophysical Journal International*, 222, 153-168. https://doi.org/10.1093/gji/ggaa153

Di Stefano, R., Chiarabba, C., Chiaraluce, L., Cocco, M., De Gori, P., Piccinini, D., & Valoroso, L. (2011). Fault zone properties affecting the rupture evolution of the 2009 (Mw 6.1) L'Aquila earthquake (central Italy): Insights from seismic tomography. *Geophysical Research Letters*, *38*(10). https://doi.org/10.1029/2011gl047365

de Kool, M., Rawlinson, N., and Sambridge, M. (2006). A practical grid based method for tracking multiple refraction and reflection phases in 3D heterogeneous media. *Geophysical Journal International*, 167, 253-270.

Ellsworth, W. L. (2013). Injection-induced earthquakes. *Science*, 341, 142–149.

Frohlich C, Hayward C, Stump B, & Potter E. (2011). The Dallas-Fort Worth earthquake sequence: October 2008 through May 2009. *Bull. Seismol. Soc. Am.*, 101:327–40

Gischig, V. S. (2015). Rupture propagation behavior and the largest possible earthquake induced by fluid injection into deep reservoirs. *Geophysical Research Letters*, 42, 7420-7428. doi:10.1002/2015GL065072

Gupta, H. K. (2002). A review of recent studies of triggered earthquakes by artificial water reservoirs with special emphasis on earthquakes in Koyna, India. *Earth-Science Reviews*, *58*(3-4), 279–310. https://doi.org/10.1016/S0012-8252(02)00063-6

He, L., Sun, X., Yang, H., Qin, J., Shen, Y., & Ye, X. (2018). Upper crustal structure and earthquake mechanism in the Xinfengjiang Water Reservoir, Guangdong, China. *Journal of Geophysical Research: Solid Earth*, 123. https://doi.org/10.1029/2017JB015404

Horton S. (2012). Disposal of Hydrofracking Waste Fluid by Injection into Subsurface Aquifers Triggers Earthquake Swarm in Central Arkansas with Potential for Damaging Earthquake. Seismological Research Letters, 83(2), 250-260.

Hunter, J. D.: Matplotlib: A 2D Graphics Environment. *Computing in Science & Engineering*, *9*(3), (2007), 90-95.

Keranen, K. M., H. M. Savage, G. A. Abers, & E. S. Cochran. (2013). Potentially induced earthquakes in Oklahoma, USA: Links between wastewater injection and the 2011 Mw 5.7 earthquake sequence. *Geology*, 2011-2014, G34045, doi:10.1130/G34045.1.

Keranen, K. M. & Weingarten, M. (2018). Induced Seismicity. *Annual Review of Earth and Planetary Sciences*, 46, 149-174.

Langenbruch, C., & M. D. Zoback. (2016). How will induced seismicity in Oklahoma respond to decreased saltwater injection rates?. *Sci. Adv., 2*(11), e1601542. doi:10.1126/sciadv.1601542

Lei, J., & D. Zhao. (2009). Structural heterogeneity of the Longmenshan fault zone and the mechanism of the 2008 Wenchuan earthquake (Ms 8.0). *Geochem. Geophys. Geosyst.*, 10, Q10010. doi:10.1029/2009GC002590

Lin, G., & Shearer, P. M. (2007). Estimating Local Vp/Vs Ratios within Similar Earthquake Clusters. *Bulletin of the Seismological Society of America*, 97(2), 379-388. doi:10.1785/0120060115

Lin, G., & Shearer, P. M. (2009). Evidence for water-filled cracks in earthquake source regions. *Geophysical Research Letters*, 36, L17315. https://doi.org/10.1029/2009GL039098

McMahon, N. D., R. C. Aster,W. L. Yeck, D. E. McNamara, & H. M. Benz. (2017). Aftershock catalog for the November 2011 Prague, Oklahoma, earthquake sequence, U.S. Geol. Surv. Data Release, doi:10.5066/F7FJ2FNT.

Pei, S., Peng, Z., & Chen, X. (2018). Locations of injection-induced earthquakes in Oklahoma controlled by crustal structures. *Journal of Geophysical Research: Solid Earth, 123*, 2332-2344. https://doi.org/10.1002/2017JB014983

Pennington C.N., Chen X., Abercrombie R.E., & Wu Q. (2021). Cross Validation of Stress Drop Estimates and Interpretations for the 2011 Prague, OK, Earthquake Sequence Using Multiple Methods. *Journal of Geophysical Research: Solid Earth*, 126, e2020JB020888. https://doi.org/10.1029/2020JB020888

Petersen MD, Mueller CS, Moschetti MP, Hoover SM, Llenos AL, et al. (2016). Seismic-hazard forecast for 2016 including induced and natural earthquakes in the central and eastern United States. *Seismol. Res. Lett.*, 87:1327-1341

Petersen MD, Mueller CS, Moschetti MP, Hoover SM, Shumway AM, et al. (2017). 2017 One-Year Seismic-Hazard Forecast for the Central and Eastern United States from Induced and Natural Earthquakes. *Seismol. Res. Lett.*, 88:772-783

Petersen MD, Mueller CS, Moschetti MP, Hoover SM, & Rukstales KS. (2018), 2018 One-Year Seismic Hazard Forecast for the Central and Eastern United States from Induced and Natural Earthquakes. *Seismol. Res. Lett.*, 89:1049-1061

Pollyea, R.M., Chapman, M.C., Jayne, R.S., & Wu, H. (2019). High density oilfield wastewater disposal causes deeper, stronger, and more persistent earthquakes. *Nature communications, 10*(1), 1-10.

Qin, Y., Chen, X., Walter, J. I., Haffener, J., Trugman, D. T., Carpenter, B. M., et al. (2019). Deciphering the stress state of seismogenic faults in Oklahoma and southern Kansas based on an improved stress map. *Journal of Geophysical Research: Solid Earth*, *124*(12), 12920-12934. https://doi.org/10.1029/2019JB018377

Rawlinson, N., Kool, M. D., & Sambridge, M. (2006). Seismic wavefront tracking in 3D heterogeneous media: Applications with multiple data classes. *Exploration Geophysics*, *37*(4), 322–330. https://doi.org/10.1071/eg06322

Takei, Y. (2002). Effect of pore geometry on Vp/Vs: From equilibrium geometry to crack. *Journal of Geophysical Research*, *107*(B2), 2043. https://doi.org/10.1029/2001JB000522

Tan, Y., Hu, J., Zhang, H., Chen, Y., Qian, J., Wang, Q., et al. (2020). Hydraulic fracturing induced seismicity in the southern Sichuan Basin due to fluid diffusion inferred from seismic and injection data analysis. *Geophysical Research Letters*, 47. https://doi.org/10.1029/2019GL084885

Schultz R, Corlett H, Haug K, Kocon K, MacCormack K, et al. (2016). Linking fossil reefs with earthquakes: geologic insight to where induced seismicity occurs in Alberta. *Geophys. Res. Lett*., 43:2534-42

Shah, A. K., & Keller, G. R. (2017). Geologic influence on induced seismicity: Constraints from potential field data in Oklahoma. *Geophysical Research Letters*, 44, 152-161. https://doi.org/10.1002/2016GL071808

Shah, A. K., & Crain, K. (2018). Aeromagnetic Data Reveal Potential Seismogenic Basement Faults in the Induced Seismicity Setting of Oklahoma. *Geophysical Research Letters*, 45, 5948-5958. https://doi.org/10.1029/2018GL077768

Shearer, P. M. (1988). Cracked media, Poisson's ratio, and the structure of the upper oceanic crust. *Geophys. J.*, 92, 357- 362.

Stewart FL, & Ingelson A. (2017). Regulating energy innovation:US responses to hydraulic fracturing, wastewaterinjection and induced seismicity. *J. Energy Nat. Resour. Law*, 35:109-46

Sumy, D.F., Cochran, E.S., Keranen, K.M., Wei, M., & Abers, G.A. (2014). Observations of static Coulomb stress triggering of the November 2011 M 5.7 Oklahoma earth-quake sequence. *J. Geophys. Res., Solid Earth*, 119, 1904-1923.

Sumy, D. F., Neighbors, C. J., Cochran, E. S., & Keranen, K. M. (2017). Low stress drops observed for aftershocks of the 2011 M w 5.7 Prague, Oklahoma, earthquake. *Journal of Geophysical Research: Solid Earth*, *122*(5), 3813-3834. https://doi.org/10.1002/2016JB013153

Sun, X., & Hartzell, S. (2014). Finite-fault slip model of the 2011 Mw 5.6 Prague, Oklahoma earthquake from regional waveforms. *Geophysical Research Letters*, *41*(12), 4207-4213. https://doi.org/10.1002/2014GL060410

Yeck, W. L., M. Weingarten, H. M. Benz, D. E. Mcnamara, E. Bergman, R. B. Herrmann, J. Rubinstein, & P. S. Earle. (2016). Far-field pressurization likely caused one of the largest injection induced earthquakes by reactivating a large pre-existing basement fault structure. *Geophys. Res. Lett.*, *43*(10),198-10,207. doi:10.1002/2016GL070861

Yeo, I. W., Brown, M. R. M., Ge, S., & Lee, K. K. (2020). Causal mechanism of injection-induced earthquakes through the Mw 5.5 Pohang earthquake case study. *Nature Communications*, *11*(1), 2614. https://doi.org/10.1038/s41467-020-16408-0

Waldhauser, F., & Ellsworth, W. L. (2000). A doubleDifference earthquake location algorithm: Method and application to the northern Hayward fault, California. *Bulletin of the Seismological Society of America*, *90*(6), 1353-1368. https://doi.org/10.1785/0120000006

Walsh, F., & Zoback, M. D. (2015). Oklahoma's recent earthquakes and saltwater disposal. *Science Advances*, *1*(5), e1500195. https://doi.org/10.1126/sciadv.1500195

Wessel, P., Luis, J. F., Uieda, L., Scharroo, R., Wobbe, F., Smith, W. H. F., & Tian, D. (2019). The Generic Mapping Tools version 6. Geochemistry, Geophysics, Geosystems, 20, 5556–5564. https://doi.org/10.1029/2019GC008515

474 Wu, Q., Chapman, M., & Chen, X. (2018). Stress-drop variations of induced earthquakes in
475 Oklahoma. *Bulletin of the Seismological Society of America*, *108*(3), 1107-1123.
476 https://doi.org/10.1785/0120170335

477 Zenonos, A., DeSiena, L., Widiyantoro, S., Rawlinson, N. (2020). Direct inversion of S-P
478 differential arrival times for Vp/Vs ratio in SE Asia. *Journal of Geophysical Research: Solid*
479 *Earth*, 125, e2019JB019152. https://doi.org/10.1029/2019JB019152